Available online at www.sciencedirect.com
SCIENCE DIRECT®
Journal of Crystal Growth 282 (2005) 438–447
JOURNAL OF CRYSTAL GROWTH
www.elsevier.com/locate/jcrysgro

Effects of alginic acid from marine algae on calcium carbonate electrodeposited coating

Jorge Pavez[a,b,*], Juan F. Silva[a,b], Francisco Melo[a,b]

[a]*Laboratorio de Física No Lineal, Departamento de Física, Facultad de Ciencia, Universidad de Santiago de Chile, Casilla 307, correo 2, Santiago, Chile*
[b]*Centro para la Investigación Interdisciplinaria Avanzada en Ciencias de los Materiales CIMAT-Chile*

Received 28 April 2005; received in revised form 9 May 2005; accepted 9 May 2005
Available online 27 June 2005
Communicated by R. Giege

Abstract

The effect of alginic acid, extracted from the *Lessonia trabeculata* calcareous marine algae, was studied in the electrocrystallization of calcium carbonate ($CaCO_3$) on indium tin oxide (ITO) transparent electrodes. Scanning electron microscopy, X-ray diffraction-collected data and microscopic observations show that the presence of Mg^{2+} at the electrolyte induces the magnesium calcite and aragonite phase formation along with the changes in morphology and crystal orientation. Addition of alginic acid strongly inhibits the effect of Mg^{2+} on the crystallization, receiving in favor of the nucleation and growth of calcite phase of $CaCO_3$. These results suggest that the alginic acid acts as an organic template in the electrocrystallization of $CaCO_3$, controlling the crystallographic orientation of crystal growth, and as a consequence, the crystal morphology.

PACS: 81.10.Dn; 81.15.Pq; 83.80.Lz; 87.64.Bx; 87.64.Dz

Keywords: A2. Electrodeposit; B1. Alginate; B1. Calcite; B1. Calcium Carbonate; B1. Magnesium calcite

1. Introduction

Calcium carbonate ($CaCO_3$) in its three different phases, calcite, aragonite and vaterite, is broadly distributed in nature [1]. Calcite and Aragonite, the most stable phases of $CaCO_3$ at ambient conditions [2,3], are present in many mineralized tissues in biologic systems. This presence is achieved through a biomineralization process. This process is genetically commanded and controlled for cells that are responsible for synthesizing the biologic matrixes which permit the organisms to control the microstructure,

*Corresponding author. Laboratorio de Física No Lineal, Departamento de Física, Facultad de Ciencia, Universidad de Santiago de Chile, Casilla 307, correo 2, Santiago, Chile. Tel.: +56 2 7763322; fax: +56 2 7769596.
E-mail address: jpavez@lauca.usach.cl (J. Pavez).

0022-0248/$ - see front matter © 2005 Elsevier B.V. All rights reserved.
doi:10.1016/j.jcrysgro.2005.05.037

morphology and kinetics of crystal growth during the mineralization [4–7]. Several mechanisms have been proposed that are useful in describing the Biomineralization process; among them is the template-mediated mineralization that is a novel and well-controlled way to grow oriented inorganic phases [8]. This mechanism involves mineral nucleation and growth onto a functionalized organic structure. In many of these systems nucleation can take place on biomineral matrices [9], on 3-D structures [8] or on thin films [10,13]. Demineralization of biological tissues is a direct way to isolate macromolecules that constitute the water-insoluble component of organic matrix and provides the organic template for biomineralization. On the other hand, these water-insoluble macromolecules need to be associated with acidic water-soluble macromolecules (acidic glycoproteins and amino acids in general) obtained from the demineralization process as well and that would be controlling nucleation and orientation of inorganic phases [8]. However, some studies have shown that natural polysaccharides from the marine environment can act as organic templates under certain conditions of supersaturation, yielding the remineralization of the matrix without adding acidic water-soluble macromolecules [9,17]. For instance, Manoli et al. [9] reported the crystallization of calcium carbonate on chitin, a polysaccharide which is a major component of the exoskeletons of arthropods. This polysaccharide promoted the exclusive formation of the calcite phase of $CaCO_3$ and the rate of crystallization depending on the supersaturation level of the solution, and the amounts of chitin had no effect on the kinetic parameters. The authors suggest that calcite formation may be induced by the interaction of Ca^{2+} ions with hydroxyl groups of chitin. Using a calcium-bonding acid polysaccharide extracted from marine algae, Wada et al. [17] showed that the organic macromolecule takes control over which phase of $CaCO_3$ will be expressed depending on the amount of polysaccharide added to the solution under certain values of supersaturation of Ca^{2+} and carbonate ions. In marine environments the calcium carbonate precipitation assisted by acid polysaccharide is a common phenomenon. It can be found in the formation of mollusk shell, in the invertebrate skeletons, and in the cell wall of marine algae.

$CaCO_3$ can also be formed directly by the organisms as surface structures of the cells [8]. The alginates are polysaccharides exclusively extracted from cell walls of algae and some bacteria, and can form gels in the presence of divalent cations, such as calcium. The alginic acid is a natural polysaccharide that is found in the cell walls of a large number of species of brown seaweed, their biological functions being to provide structural support to the seaweed. It is a polysaccharide polyuronide type composed of different proportions of units of β-D-mannuronic acid and α-L-guluronic acid linked by bonds β-1 → 4 and α-1 → 4 (see Fig. 1) [2]. The proportions and sequences of these units along the polysaccharide chain vary according to the natural source, and the physical properties of alginic acid depend on these proportions and sequences, the α-L-guluronic unit being mainly responsible for the structural function of alginate in marine algaes [14,15].

The alginates have a very interesting ion-bonding property that has attracted a considerable attention and many studies focused on this property have been carried out [16]. These studies conclude that the affinity of alginates for divalent ions grows with increasing of L-guluronic residue in the polysaccharide chain, thus promoting the formation of GG-blocks in majority as compared with the MM and MG blocks (see Fig. 1). These studies also showed that when the presence of L-guloronic units is more than the D-mannuronic one, the affinity of alginates within the alkaline-earth metal ions follows the order, $Ba^{2+} > Sr^{2+} > Ca^{2+} \gg Mg^{2+}$.

Here we present a study of the effect of alginic acid extracted and isolated from the *Lessonia trabeculata* calcareous marine algae [19] on the crystal morphology of calcium carbonate electrochemically deposited on ITO electrode. The method used is based on previous works and the original idea proposed by Lédion et al. [20] described below. Our interest is to investigate whether the alginate has the capacity to act as an organic template in the electrodeposition of calcium carbonate, stimulating the orientation of crystallization even in the presence of Mg^{2+} which

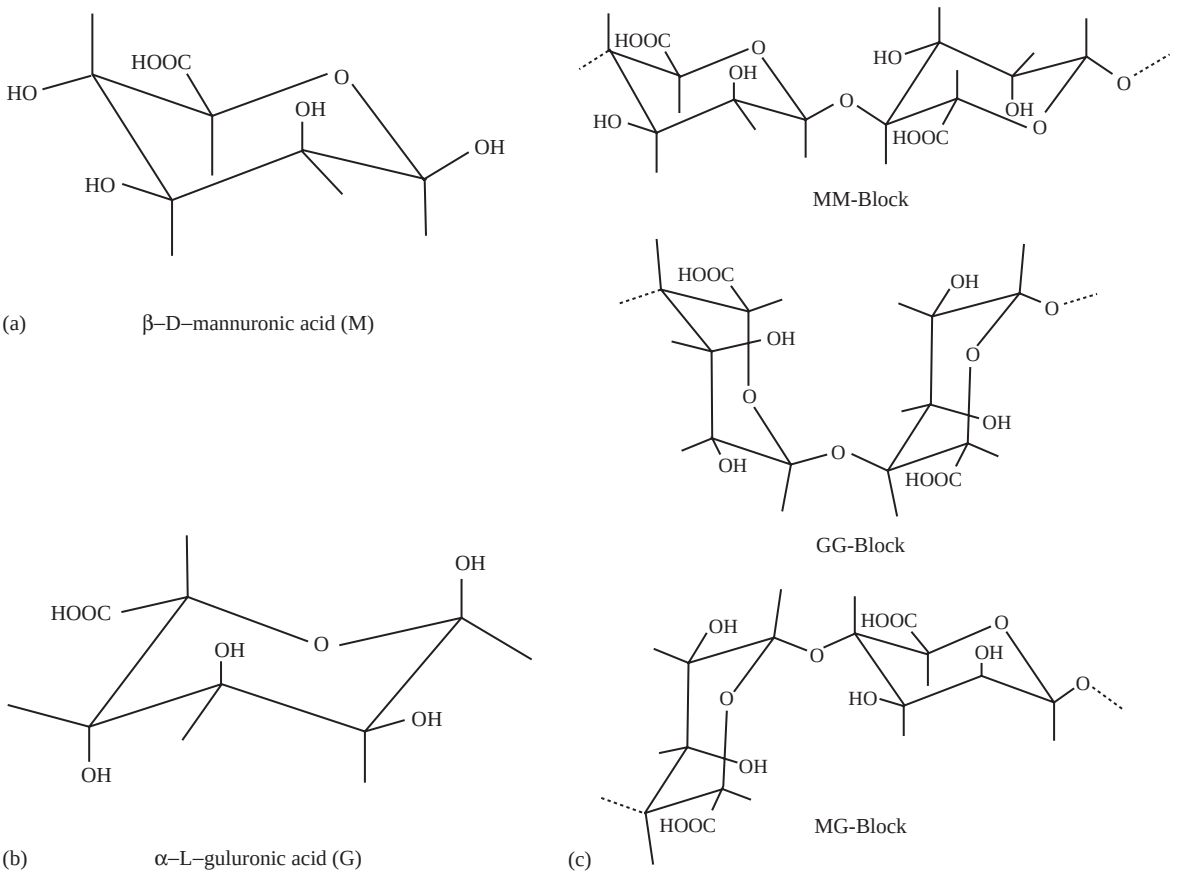

Fig. 1. Structure of alginic acid extracted from *Lessonia trabeculata* marine algae; (a) D-mannuronic residue: M, (b) L-guluronic residue: G, (c) polysaccharide chain: three different possibilities of residue bonding.

is a strong inducer of magnesium calcite and aragonite phase of calcium carbonate.

2. Materials and experimental procedure

2.1. Materials

All the electrolytes were reagent grade and were used as received; $CaCl_2$ dihydrate, $MgCI_2$ hexahydrate and $NaHCO_3$ were from Aldrich and NaCl and NaOH were from Merck. The alginic acid was extracted and isolated from the *L. trabeculata* calcareous marine algae [19]. Water used for electrolytes solutions was deionized and purified further by double distillation. Indium tin oxide (ITO, 90% In_2O_3 and 10% SnO_2) conductive glass electrodes, (Delta Technologies, USA) were cleaned with methanol and extensively rinsed with ultra-pure Milli-Q water and sonicated for 5 min prior to use. A platinum (99.99, Aldrich) spiral wire and a silver/silver–chloride (Ag/AgCl) electrode were used as auxiliary and reference electrodes, respectively. The potential values are given versus Ag/AgCl. The linear sweep voltammetry and chronoamperometric experiments were carried out in a conventional three-compartment electrochemical cell. The experiments were performed with a potentiostat/galvanostat Autolab Pgstat 30, Eco Chemie, NL. The AFM images were obtained with a commercial microscope (Nanoscope IIIa Multimode, Digital Instruments,

USA) equipped with Si_3N_4 cantilevers (Digital Instruments) with the triangular tip scanning in contact mode at a scan rate of 1.5 Hz.

2.2. Procedures and apparatus

Prior to the electrodeposition of $CaCO_3$ a linear sweep voltammogram was performed scanning the working electrode between 0 and −1.0 V at a scan rate of 5 mV/s. This procedure was carried out in order to determine the potential value where oxygen reduction reaches the maximum activity, i.e., the potential where the diffusional current is achieved, this value is −0.86 V. Calcium carbonate coating was generated by applying a constant negative potential (this is related to the choice of −0.86 V) to the ITO working electrode for two–three hours which was then submerged in $NaHCO_3$ and $CaCl_2$ solution saturated with molecular oxygen. The electrolyte solution consisted of a mixture of $CaCl_2$ (2 mM), $NaHCO_3$ (6 mM) and NaCl (10 mM). The pH was maintained at 8.25 by adding 0.1 mM NaOH. The conductive glass electrodes with crystalline coating were mounted on a scanning electron microscope (SEM) sample holder with conductive carbon paste and were sputter-coated with a thin layer of gold. The samples were examined with a JEOL (Japan) SEM model JSM 5410 and the images were obtained by observing the angle normal to the surface of the sample. The angles between crystal edges in SEM images were determined with measuring tools in SigmaScan Pro version 5 (Jandel Scientific, USA). Siemens X-ray diffractometer model D 5000 (Siemens, Germany) was used for XRD measurements in the θ–2θ mode at grazing angles.

3. Results and discussion

3.1. Electrochemically induced crystallization

The crystallization of calcium carbonate was electrochemically aided using a method proposed in 1985 by Lédion et al. [20] for the study of scaling rate. In this method, an adequate electrolyte solution with molecular oxygen (O_2) dissolved is used at alkaline pH and the electrochemical reduction of O_2 is promoted by applying a sufficiently negative potential. The electroreduction of oxygen produces a local increment of pH which in turn induces the bicarbonate ions present at the interface to become carbonate; thus, the precipitation of $CaCO_3$ is achieved.

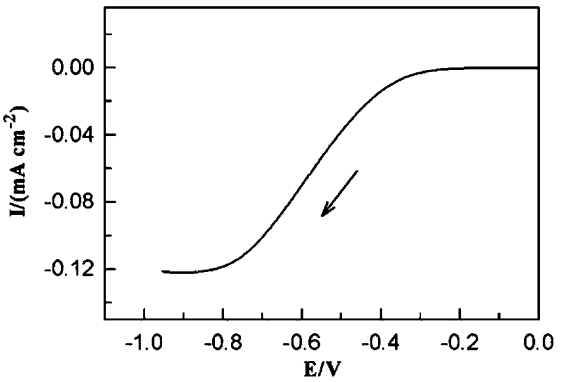

Fig. 2. Linear sweep voltammogram of O_2 reduction on ITO electrode. O_2-satured electrolyte solution: $CaCl_2$ (2 mM), $NaHCO_3$ (6 mM) and NaCl (10 mM). pH = 8.25, Scan rate 5 mV/s.

Fig. 2 shows the linear sweep voltammogram obtained for the reduction of O_2 on an ITO electrode at pH 8.25 recorded at 5 mV/s. The voltammetric response shows an irreversible cathodic wave at negative potential, which corresponds to the reduction of O_2 to peroxide by two-electron transfer [21,22]. The voltammogram of Fig. 2 shows that the value of the diffusion-limit current for the oxygen reduction is achieved at −0.86 V of applied potential. Based on this voltammetric profile, the value of −0.86 V was chosen to be applied to the ITO working electrode to promote the electrodeposition of $CaCO_3$.

3.2. Morphological analysis of crystalline coating

The crystalline coatings, once obtained, were analyzed using optical and scanning electron microscopy and, X-ray diffraction in the θ–2θ scan mode. From the data collected the predominant crystallographic orientations were determined. Figs. 3 and 4 show representative scanning electron micrographs and XRD patterns

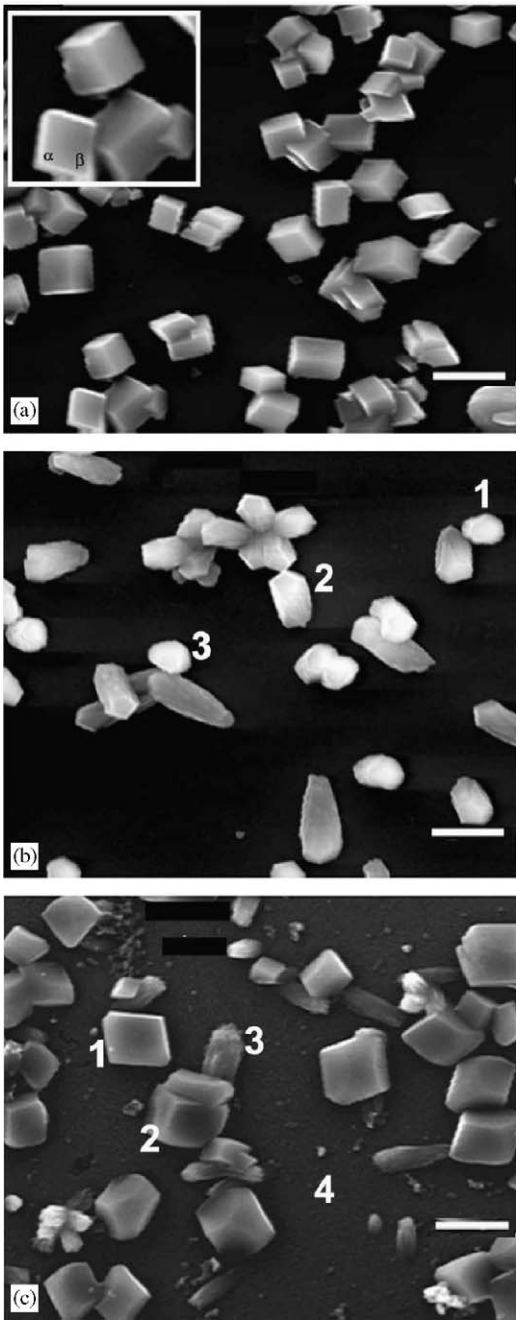

Fig. 3. Scanning electron micrograph of calcium carbonate crystals electrodeposited onto ITO electrode from the O_2-satured electrolyte containing: (a) ($CaCl_2$) 2 mM, ($NaHCO_3$) 6 mM and (NaCl) 10 mM. (b) ($CaCl_2$) 2 mM, ($NaHCO_3$) 6 mM, (NaCl) 10 mM and ($MgCI_2$) 1 mM. (c) ($CaCl_2$) 2 mM, ($NaHCO_3$) 6 mM, (NaCl) 10 mM, ($MgCI_2$) 1 mM and alginic acid 10 mg/L. Scale bar = 10 μm.

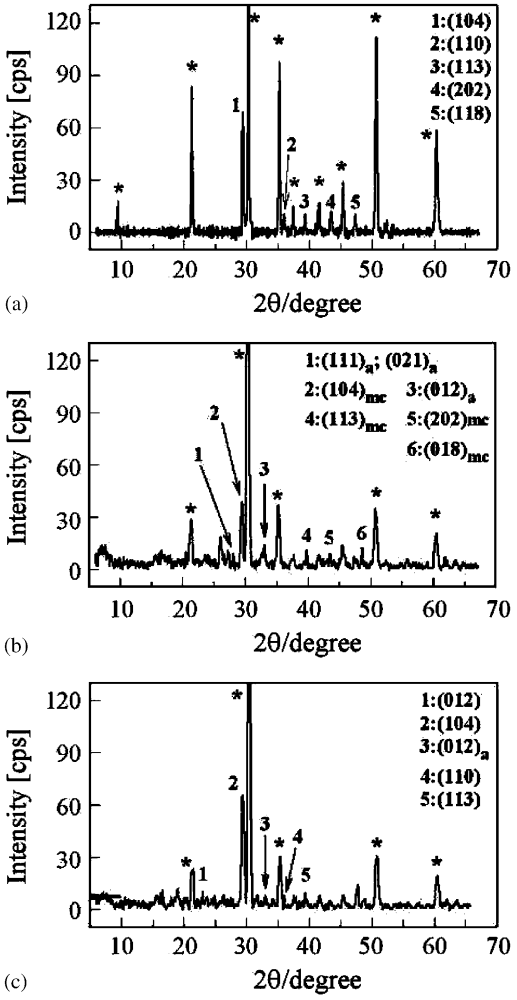

Fig. 4. X-ray diffraction data of calcium carbonate electrocrystallized on an ITO electrode for 3 h at −0.86 V, from the O_2-satured electrolyte containing: (a) ($CaCl_2$) 2 mM, ($NaHCO_3$) 6 mM and (NaCl) 10 mM. (b) ($CaCl_2$) 2 mM, ($NaHCO_3$) 6 mM, (NaCl) 10 mM and ($MgCI_2$) 1 mM. (c) ($CaCl_2$) 2 mM, ($NaHCO_3$) 6 mM, (NaCl) 10 mM, ($MgCI_2$) 1 mM and alginic acid 10 mg/L. Subindexes a, c and, mc indicate aragonite, calcite and magnesium calcite peaks, respectively.

respectively, of ITO electrodes after the electrodes position of calcium carbonate under the described conditions. The crystalline coating in Fig. 3a and its XRD spectra in Fig. 4a correspond to the control experiment, i.e. crystallization conditions without the additives used in this study: Mg^{2+} and

alginate. Thus, the crystalline deposit obtained is constituted by crystals of calcite with very well-established rhombohedral equilibrium morphology with {1 0 4} faces and about 8 μm in average size. The rhombohedral calcite crystals grew with a certain degree of homogeneous distribution upon the surface electrode and with preferred orientations. The angles α and β of the zoomed SEM view in the inset of Fig. 3a (corresponding to the crystal located at the right bottom of the image) define the crystallographic orientation of the rhombohedral crystal [10,12]. Thus, the angles' values, $\alpha = 102^\circ$ and $\beta = 78^\circ$, of the flat rhombohedral crystal unequivocally identify the (1 0 4) crystallographic plane according to the known structural data of the calcite unit cell [10,12]. The XRD spectra displayed in Fig. 4a confirm that rhombohedral crystals predominantly grow from (1 0 4) crystallographic planes, as is evidenced by the strong diffraction peak at 2θ equal to 29.4°, and there are four other weaker diffraction peaks at36.0°, 39.4°, 43.3°, 47.4° 2θ values which are produced by (1 1 0), (1 1 3), (2 0 2) and (1 1 8) crystallographic nucleation planes of calcite phase of calcium carbonate, respectively [10,12]. The SEM and X-ray information indicate that there is no face-selective nucleation for the electrocrystallization on ITO electrode, i.e., this kind of oxide mixture surface does not induce a preferred orientation for calcite nucleation. The peaks labelled "*" in XRD spectra correspond to signals due to the ITO substrate [23,24].

When the Mg^{2+} is added to the electrolyte (in a $Mg^{2+}/Ca^{2+} = 0.5$ molar ratio) the crystalline deposit evidences a drastic change in its morphology and size as can be seen in Fig. 3b. The deposit showed individual and star-shaped crystals as aggregated. The influence of magnesium on crystal morphology is clearly seen and the crystals elongate in the direction of the *c*-axis and truncated rhombohedra crystals. The presence of Mg^{2+} within the crystallization media of calcium carbonate exerts a strong influence on the nucleation and growth, and induces the appearance of magnesium-calcite (Mg-calcite) in addition to the aragonite phase depending on the Mg^{2+}/Ca^{2+} molar ratio [8,12]. Low Mg-calcite (<4 mol% of magnesium) precipitates when the ratio is $\leqslant 1$, whereas at ratio values >1 high Mg-calcite (>4 mol% of magnesium) will precipitate, which is less stable than low Mg-calcite. In the literature, there are two principal reported mechanisms by which magnesium modifies the crystal growth of calcium carbonate, and they are still being researched. One of the mechanisms suggests that the magnesium contaminate the calcite nuclei by Mg^{2+} adsorption at the active growth sites on specific faces [25,26], and in the other one Mg^{2+} retards the crystallization of calcium carbonate by incorporating itself into the calcite crystal and replacing the Ca^{2+} in the lattice [27,28].

The X-ray diffraction data of Fig. 4b, which correspond to the crystalline coating obtained in the presence of magnesium in the electrolyte, indicate that two phases of $CaCO_3$ are present at coating; magnesium calcite and aragonite, the first being the major one as the strongest peaks are from the magnesium calcite phase. The diffraction lines at 2θ equal to 26.5°, 27.2° and 33.1° correspond to (1 1 1), (0 2 1) and (0 1 2) aragonite peaks, respectively. Moreover, the signals at 2θ equal to 29.7°, 39.8°, 43.5° and, 48.3° those corresponding to (1 0 4), (1 1 3), (2 0 2) and (0 1 8) crystallographic planes, respectively, are generated from magnesium calcite phase [10,12]. Energy-dispersive X-ray scattering analysis (EDXS) showed that there is a direct relationship between the crystal morphology changes and the magnesium content when this element was added to electrolyte. The magnesium contents of crystals 1, 2, and 3 in Fig. 3b are 3.01 mol% 2.38 and 2.59 mol%, respectively. The rounded shapes of the crystals seen (numbers 1 and 3) results from a higher Mg content than the striated facets and elongated crystals (number 2), the former probably corresponding to the magnesium calcite phase [8,10–12]. Although the Mg contents did not show very significant differences, the X-ray diffraction data along with the SEM and EDXS information strongly suggest that Mg^{2+} is adsorbed onto specific faces of calcite crystal and, in parallel and in a more important manner magnesium is incorporated into the $CaCO_3$ crystal lattice, inducing the expression of the magnesium calcite phase [28–30].

A drastic change in the situation described above takes place when the electrocrystallization is performed when alginic acid is present in the electrolyte besides Mg^{2+} ion, as shown in the SEM image of Fig. 3c and the X-ray spectra in Fig. 4c. The size, morphology, and shape of crystals showed a large variation and button-like characteristics of the surface electrode. Despite the presence of Mg^{2+} ion, the crystalline structures displayed in Fig. 3c show a rhombohedral equilibrium morphology with a predominant expression of {1 0 4} faces with about 10 μm in average size. According to these experimental conditions, the alginic acid is responsible for these changes. The orientations of crystals were estimated in using both X-ray data and SEM micrographs. The group of {1 0 4} rhombohedral faces is confirmed by a very strong (1 0 4) peak at 2θ equal to 29.4° along with three weaker peaks at 2θ equal to 23.03°, 36.0° and, 39.4° that correspond to (0 1 2), (1 1 0) and (1 1 3) crystallographic planes, respectively which were generated from calcite phase. For action of alginic acid, the signals at X-ray spectra corresponding to the other $CaCO_3$ phases generated in the presence of Mg^{2+} ion, almost completely disappeared, with just one weak signal remaining for aragonite (0 1 2). The EDXS analysis for magnesium contents indicated that crystals 1, 2, and 3 in Fig. 3c have 0.0, 0.0 and 5.37 mol%, respectively. These results match with X-ray data and SEM micrographs showing that there was no incorporation of Mg^{2+} ion within the crystal lattice of calcite nuclei. Thereby, the alginate would be protecting calcite nuclei from two adverse events: Mg^{2+} adsorption onto the specific faces of calcite, and the substitution of calcium by magnesium within the crystal lattice that promotes the magnesian calcite phase. This experimental information strongly suggests that alginic acid plays an important role during the electrocrystallization of $CaCO_3$, which would correspond to an organic template. This role is accomplished thanks to ion-bonding property specifically directed Ca^{2+}.

The naturally extracted alginic acid used in this study corresponds to a mixture of units of β-D-mannuronic acid and α-L-guluronic (G) acid with a ratio $M/G = 0.46$. This means that in a solution of this biopolymer the probability of finding GG-block residues bonding is greater than the MM-block or MG-block. In agreement with data found in the literature the homopolymer GG-block is the best structure of alginic acid for the calcium ion-bonding property. This organic architecture confers the polysaccharide into a specially ordered and charged structure for bonding calcium ion selectively instead of magnesium during the first stages of nucleation. This special interfacial property is achieved on the basis of a stereochemical arrangement of the carboxylate and hydroxyl functional groups of the G units in the GG-blocks, allowing a certain level of molecular recognition at the organic template–mineral interface. The negative charged zone and the spatial dimensions within the compartment confirmed by GG-blocks induces the nucleation of calcium by a phenomenon called Ionotropic nucleation. Once the first layers of calcium ion are confined within the polysaccharide blocks specifically linked to carboxylate groups, carbonate ions are linked to calcium and therefore the nucleation processes take place aided by alginate. Thereby, there is a face-selective nucleation process on the (1 0 4) plane of calcite.

As mentioned above, it can be noticed from image 3c that after the electrochemical deposition was performed in the electrolyte containing calcium, magnesium and bicarbonate ions along with alginic acid, the base of the surface electrode shows a particular morphology. In Fig. 3c a layer-structured material is observed that lies on the base of the electrode surface where the crystals recide. Later, an experiment was conducted to know whether this material that reaches at the base of the electrode corresponds to an insoluble species precipitated along with calcium ion during the electrodeposition process but prior to the nucleation. The microscope image in Fig. 5a shows the surface of ITO's pristine electrode captured after performing a chronoamperometric experiment on the electrolyte support, i.e., without the calcium and magnesium ions. No coating was observed on the surface in those conditions. This situation is also observed when the magnesium ion and alginic acid are added into the electrolyte (see image 5b). This is confirmed by the X-ray data

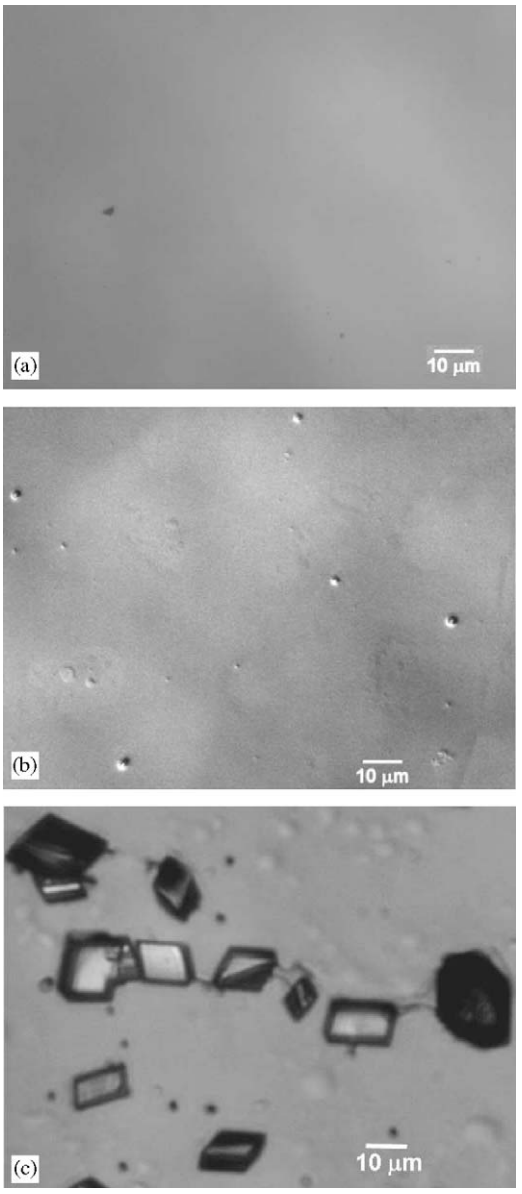

Fig. 5. Microscope images of coating electrodeposited onto an ITO electrode from a O_2 satured electrolyte containing: (a) ($NaHCO_3$) 6 mM and (NaCl) 10 mM. (b) ($NaHCO_3$) 6 mM, (NaCl) 10 mM, ($MgCI_2$) 1 mM and alginic acid 10 mg/L. (c) ($NaHCO_3$) 6 mM, (NaCl) 10 mM, ($CaCl_2$) 2 mM and, alginic acid 10 mg/L.

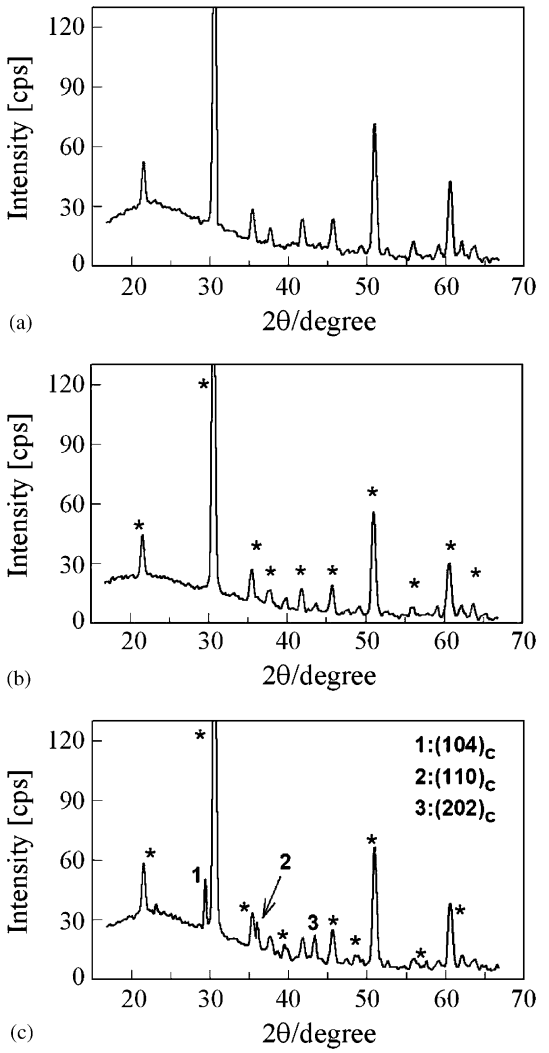

Fig. 6. X-ray diffraction data of coatings electrodeposited onto an ITO electrode from the O_2-satured electrolyte containing: (a) ($NaHCO_3$) 6 mM and (NaCl) 10 mM. (b) ($NaHCO_3$) 6 mM, (NaCl) 10 mM, ($MgCI_2$) 1 mM and alginic acid 10 mg/L. (c) ($CaCl_2$) 2 mM, ($NaHCO_3$) 6 mM, (NaCl) 10 mM, and alginic acid 10 mg/L. Peaks labelled "*" correspond to ITO substrate signals.

shown in Fig. 6 in the spectra labelled a and b. The X-ray pattern is similar for both surfaces, and therefore there is no evidence of any deposit on the electrode surface. The situation is very different when the experiments are carried out with calcium ion and alginic acid incorporated into the electrolyte support. The image in Fig. 5c and the X-ray spectrum displayed in Fig. 6c clearly show that crystalline coating is only achieved when the

electrodeposition is achieved in the presence of calcium ion in the electrolyte, and the crystalline phase of the $CaCO_3$ deposited corresponds to calcite. At the surface sector labelled as the number 4 in Fig. 3c the content of magnesium is 0.0% and the calcium content is 28.68%.

Imaging the electrode surface before and after electrocrystallization of $CaCO_3$ in the presence of the additives used in this study can aid in the visualization of the material layer-structured film that lies at the base of the electrode surface in more detail. The AFM image (displaying deflection signal) in Fig. 7a represents the surface of a pristine electrode captured in the electrolyte prior to electrocrystallization. The principal feature of this surface is its granular and homogeneous conformation with a surface roughness of about 3 nm (root mean square surface roughness (RMS)) [31,32]. The AFM image in Fig. 7b represents the morphology of the layer-structured material around the surface sector labelled no. 4 in Fig. 3c, after the electrochemical deposition of calcium carbonate in the presence of the additives. This image shows a porous and fibrous structure that grew, developing an array like a network. This structure likely corresponds to the insoluble calcium–alginate layer of the organic template. Finally, we wish to emphasize that this film structure is formed only when the calcium ion and the alginic acid are present in the electrolyte. However, more experimental tests are required to fully characterize the mechanical and chemical properties of the film, especially the existence of the calcium II–alginate complex coordination.

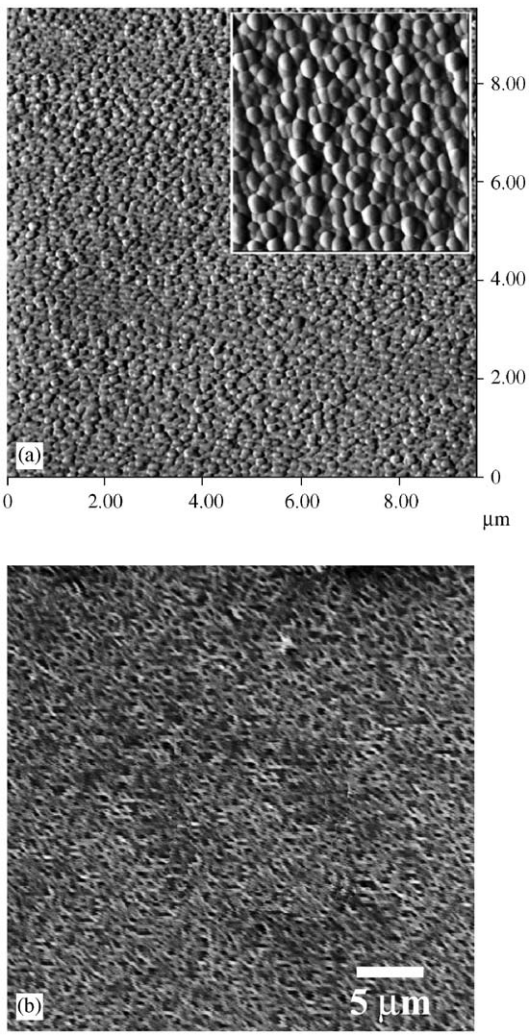

Fig. 7. (a) AFM image of bare a ITO electrode. The inset image is 5 × 5 µm. (b) Bottom ITO AFM image of the electrode after the electrodeposition of calcium carbonate from the O_2-satured electrolyte containing ($CaCl_2$) 2 mM, ($NaHCO_3$) 6 mM, (NaCl) 10 mM and ($MgCI_2$) 1 mM and alginic acid 10 mg/L.

4. Conclusion

The experimental results show that the alginic acid extracted and isolated from the *Lessonia trabeculata* calcareous marine algae template indicates nucleation and growth of an electrodeposit of calcium through a highly controlled preferred crystalline orientation. This role would likely corresponds to an organic template that orients the nucleation of $CaCO_3$ towards the formation of the calcite phase. This role can be accomplished thanks to the ion-bonding property of the alginate class used here specifically with Ca^{2+} ions, which allow an Ionotropic nucleation to take place. This template effect is maintained even in the presence of a strong inductor of magnesian calcite and aragonite phase such as the Mg^{2+} ion.

Acknowledgements

J.P is grateful to Fondecyt (Chile) for Post-Doctoral project (Grant 3010009). Financial support from FONDAP-Chile (Grant 11980002) is gratefully acknowledged.

References

[1] K. Simkiss, Am. Zool. 24 (1984) 847.
[2] L.N. Plumber, E. Busenberg, Geochim, Cosmochim. Acta 46 (1982) 1011.
[3] G. Wolf, C. Günther, J. Therm. Anal. Cal. 65 (2001) 687.
[4] A.M. Belcher, X.H. Wu, R.J. Christensen, P.K. Hansma, G.D. Stucky, D.E. Morse, Nature 381 (1996) 56.
[5] S. Mann, Nature 365 (1993) 499.
[6] Y. Kitano, N. Kanamori, A. Tokuyana, Am. Zool. 9 (1969) 681.
[7] G. Falini, S. Albeck, S. Weiner, L. Addadi, Science 271 (1996) 67.
[8] S. Mann, in: Biomineralization: Principles and Concepts in Bioinorganics Materials Chemistry, Oxford University Press, Oxford, 2001.
[9] F. Manoli, S. Koutsopoulos, E. Dalas, J. Crystal Growth 182 (1997) 116.
[10] D.D. Archibald, S.B. Qadri, B.P. Gaber, Langmuir 12 (1996) 538.
[11] J. Aizenberg, A.J. Black, G.M. Whitsides, J. Am. Chem. Soc. 121 (1999) 4500.
[12] E. Loste, R.M. Wilson, R. Seshadri, F.C. Meldrum, J. Crystal Growth 254 (2003) 206.
[13] B.R. Heywood, S. Rajan, S. Mann, J. Chem. Soc. Faraday Trans. 87 (1991) 735.
[14] E. Percival, R.H. McDowell, in: Chemistry and Enzymology of Marine Algal Polysaccharides, Academic Press, New York, 1967, pp. 99–124 (Chapter 5).
[15] B. Matsuhiro, D.M. Zambrano, Bol. Soc. Chil. Quim. 34 (1989) 21.
[16] O. SmidsrØd, Faraday Disc. Chem. Soc. 57 (1974) 263.
[17] N. Wada, M. Okasaki, S. Tachikawa, J. Crystal Growth 132 (1993) 115.
[19] P. Chandía, Licenciatura Thesis, Universidad de Santiago de Chile, 2000.
[20] J. Lédion, P. Leroy, J.P. Labbe, TSM Leau, July/August (1985) 323.
[21] M. Tarasevich, A. Sadkowski, E. Yeager, Oxygen electrochemistry, in: Conway, J. Bockris, E. Yeager, S. Khan, R. White (Eds.), Comprehensive Treatise of Electrochemistry, Kinetics and Mechanisms of Electrode processes, vol. 7, Plenum Press, New York, 1983, pp. 301–398 (Chapter 6).
[22] E. Yeager, Electrochim. Acta 29 (1984).
[23] X.W. Sun, H.C. Huang, H.S. Kwok, Appl. Phys. Lett. 68 (1996) 2663.
[24] J.P. Nair, R. Jayakrishan, N.B. Chaure, R.K. Pandey, Semicond. Sci. Technol. 13 (1998) 340.
[25] S. Albeck, J. Aizemberg, L. Addadi, S. Weiner, J. Am. Chem. Soc. 115 (1993) 11691.
[26] A. Gutjahr, H. Dabringhaus, R. Lacmann, J. Crystal Growth 158 (1996) 310.
[27] L. Fernández-Díaz, A. Putnis, M. Prieto, C.V. Putnis, J. Sediment. Res. 66 (1996).
[28] K.J. Davis, P.M. Dove, J.J. De Yoreo, Science 290 (2000) 1134.
[29] S. Xu, C.A. Melendres, J.H. Park, M.A. Kamrath, J. Electrochem. Soc. 146 (1999) 3315.
[30] S. Mann, Angew. Chem. Int. Ed. 39 (2000) 3392.
[31] L. Zhou, P.K.H. Ho, P.C. Zhang, S.F.Y. Li, G.Q. Xu, Appl. Phys. A 66 (1998) S643.
[32] J. Pavez, J.F. Silva, F. Melo, Electrochim. Acta 50 (2005) 3488.